Caving 2018 – Y Potvin and J Jakubec (eds)

doi:10.36487/ACG_rep/1815_45_Urbancic

Mapping cave front growth utilising the collective behaviour of seismicity and velocity fields

G Viegas *ESG Solutions, Canada*

K Bosman *ESG Solutions, Canada*

D Angus *ESG Solutions, Canada*

W de Beer *ESG Solutions, Canada*

T Urbancic *ESG Solutions, Canada*

Abstract

In many block caving operations, the expansion and growth of the cave involves an examination of the distribution of seismicity both spatially and temporally around the cave itself. These approaches utilise event density as a proxy to define the volume of fractured rock mass and provide a 'sense' of cave front migration. However, seismic records contain a wealth of information not only about the location of fractures, but the volume encompassing the fractures (source volume) and the relative stress state of the rock mass surrounding the caving operation with distance from the cave itself. This leads to considering that observed seismicity is part of a collective response of the rock mass due to mining. We suggest that event occurrence is related to the dynamic stress conditions associated with the caving operation. In this manner, we can consider the collective behaviour of seismicity, specifically the energy and stress release states, and map, along with velocity variations, the degree of fracturing relative to the cave boundary. Here, we provide examples of how these approaches enhance our understanding of block caving and the growth of the caving front in space and time. Specifically, we identify how stress can be tracked ahead of the observed event distribution clouds and the relative degree of fracturing that occurs in the highly stressed zone.

Keywords: *cave growth, fractures, collective response, stress release, stress tracking*

1 Introduction

The effectiveness of block caving operations is directly related to the upward growth of the cave at a rate that allows for the drawdown of the collapsed zone. The success of block caving operations depends very much on being able to initiate a fracture zone that allows for the progressive growth of the cave under a relatively stable stress regime. By identifying the fracture and stress state of the volume of rock that will eventually be caved, it may be possible to guide operational actions during the extraction of ore.

Microseismic monitoring is an approach that is commonly used to track the fracture state of the cave back. Most seismic-based analyses constrain themselves to an examination of event locations or the density of events and their proximity to the cave back over time. Such an approach, although giving us an indication of where the rock is responding to caving and where stress is concentrating, does not provide details on the fracture complexity and the distribution of the fracture network. However, as shown by Westman et al. (2012), Ma et al. (2016), Mercier et al. (2015), and others, by tracking velocity variations in space and time we can monitor the stability of the rock mass during caving. An increase in stress in a rock mass promotes the closing of microcracks and pore spaces, increasing the stiffness of the rock mass, and thus resulting in an increase in the seismic velocities. Areas of decreasing seismic velocities can be interpreted as de-stressed regions and/or areas where the rock is damaged or has failed, and an increasing number of cracks are present.

We can also use microseismic events and their signals as a proxy for defining rock deformation and understanding of the stress behaviour occurring in the cave back or in the volumes surrounding the caves themselves, such as in the abutments. This can be achieved by characterising the collective behaviour of seismicity (Riznichenko 1965; Kostrov & Das 1988; Ben-Zion 2008). To quantify the collective behaviour means quantifying the nature of the events in space and time by identifying similarities in event source and signal characteristics and grouping those events in a manner so as to represent an underlying rock behaviour. The premise of this approach is based on the concept that the observed seismicity is a consequence of the underlying stress field and the changes in stress 'flow' are captured in the seismicity. This allows us to highlight different stress, fracture and deformation states within the rock mass and estimate the strength of the rock mass, how it deforms under load, and the stress field responsible for the observed seismicity (Urbancic et al. 2015).

This approach, referred to as dynamic parameter analysis (DPA), has been shown to define changes in stress and deformation behaviour associated with rockburst occurrences in hard rock mines (e.g. Smith-Boughner et al. 2017) and the fracture and stress conditions related to hydraulic fracturing of an injection borehole (see Urbancic et al. 2015; Ardakani et al. 2018). In this study, we examine data from a block caving extraction and utilise passive tomographic approaches integrated with DPA to effectively define the varying deformation associated with the cave back (fracture state) and stress behaviour associated with the caving operation.

We utilise the findings to develop a workflow to describe the spatio-temporal behaviour pattern and discuss the potential for utilising these approaches to track the cave front in near real-time. To develop these approaches, two case studies are considered. In the first instance, we examine the response of the rock over a two-week period and consider how these approaches can provide insight into the stress behaviour associated with caving. As a second example, we compare the integrated tomography and DPA observations to observed cave back location as identified through drilling. Using the velocity and DPA observations, we discuss a potential relationship between event occurrences and the observed changes in identified stress behaviour.

2 Approach

2.1 Travel time tomography

During caving operations, microseismic event locations and their source characteristics, e.g. energy and stress release, moment, and magnitude are obtained and can be used to get a sense of rock behavioural changes as related to caving. Additionally, measured travel times of seismic signals (microseismic events and blasts) from sources to the sensors are used for travel time tomography to image seismic velocities (P- and S-waves) in the rock volume sampled by the source–sensor paths. The temporal variation in observed velocities allows for comparisons between rock volumes experiencing significant velocity changes that characterise the stress and deformation changes surrounding the cave. To achieve this, the rock is discretised into a grid of 3D volume elements and the observed ray paths associated with the volume elements in which they occur. Operational timelines (mine activity) and large seismic events are used to define sequential time windows for the analysis of pre-deformation versus post-deformation conditions.

As a starting velocity model, a 1D background velocity (half-space) is defined over a regularly spaced 3D grid. Initial inputs for the tomographic inversion are observed travel times for blasts and microseismic events, which are used to determine the velocity perturbation for each cell with sufficient ray path coverage in the chosen grid of volume elements. Continued tracking of velocity changes uses the ray paths of subsequent blasts and microseismic events. Figure 1 shows an example of the ray paths and volumes sampled for a single time window of one week.

Our approach is based on a variant of the simultaneous iterative reconstruction technique (SIRT; see Crowley et al. 2015), which provides a computationally efficient method of solving the velocity perturbations across the grid. To simplify the analysis, we do not consider complex ray paths that diffract around the cave; instead, we utilise the simpler ray paths to minimise the introduction of errors into the velocity determinations. This selection criteria only rejects ray paths to a couple of sensors per event, since most of the ray paths are upwards and not lateral, or downwards and crossing the cave, and their exclusion will have a negligible effect on the resolution of the velocity field around the cave. Grid spacing is chosen to reflect the expected minimum scale length that is resolvable given the input waveform data. The minimum anomaly size which ray-theoretical travel times are sensitive to is equal to half the width of the Fresnel zone (Nolet 2008), which can be calculated using representative values of dominant frequency and source–sensor distance for the dataset being studied. For the current example, we obtain a minimum scale length of approximately 40 m.

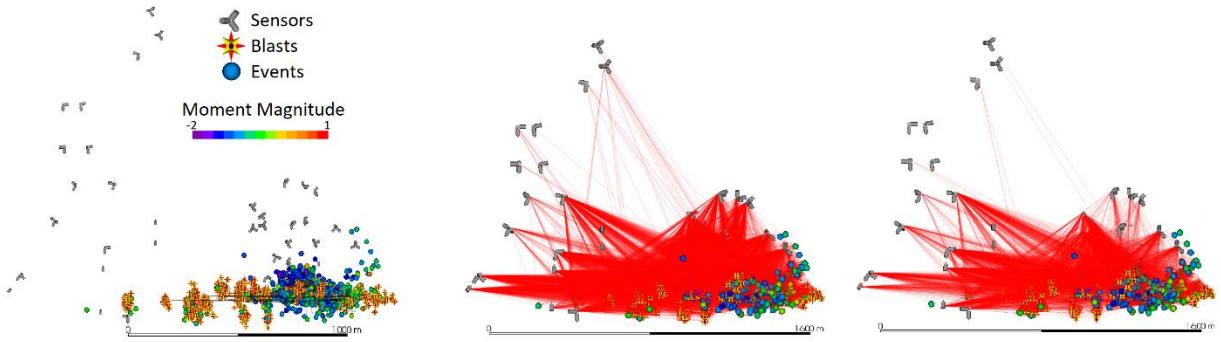

Figure 1 Three component geophone network surrounding the block cave operation along with seismicity scaled by moment magnitude. Ray path coverage of P- and S-waves (left and right, respectively) for events originating in the vicinity of the cave, showing a significant crossing of ray paths

2.2 Resolution

It is generally understood that volumes rich in ray paths crossing from different trajectories result in better resolution as compared to volumes where ray paths originate from a single direction. As shown in Figure 1, the seismic array surrounds the cave operation. From the observed distribution of seismic events, ray paths are generated from the event locations to the sensors. In the vicinity of the cave, there is a dense crossing of rays providing for a robust determination of velocities in this region. To understand the effects of resolution imposed by the ray geometry on the calculated velocities more succinctly, a checkerboard test is used (see Rawlinson & Sambridge 2003 for a discussion of this methodology), which provides a sense of the confidence level associated with the inversion results. The test consists of a synthetic model of travel times with alternating blocks of increasing and decreasing velocities. When these synthetic travel times are inverted, areas that recover the input synthetic model are said to be well resolved, and areas that do not are said to be poorly resolved. Smearing effects resulting from poorly constraining ray geometry are also easily observed near the edges of the recovered checkerboard images. To further test the robustness of the inversions, random arrival time picking errors are added to the input travel times. The size of the checkerboard pattern used in the resolution test is roughly double the expected minimum resolvable scale based on the observed microseismic signals, and is thus expected to give a reasonable estimate of the features that can be imaged.

In Figure 2, we show a checkerboard test of P-wave velocities for ray geometries of two consecutive weekly periods in cross-sectional view. The sensor geometry remained the same in both weeks, but there was a significant increase in seismicity in the second week. In the image of the first week, corresponding to a cut plane at a horizontal coordinate transecting the cave, a positive and negative ‘check’ is well recovered. This good recovery of the initial check pattern suggests that the ray geometry for the data and sensors is adequate to recover velocities in this volume.

Areas of smearing within the checkerboard pattern are observed at distance from the cave. Because this area is outside the area of interest, we are less concerned with the ability for the inversion to image velocities here. There is an observable improvement in the resolution of the P-wave checkerboard test around the cave in week two, which results from the increase in seismicity in that period and thus from the increase in ray paths sampling that volume.

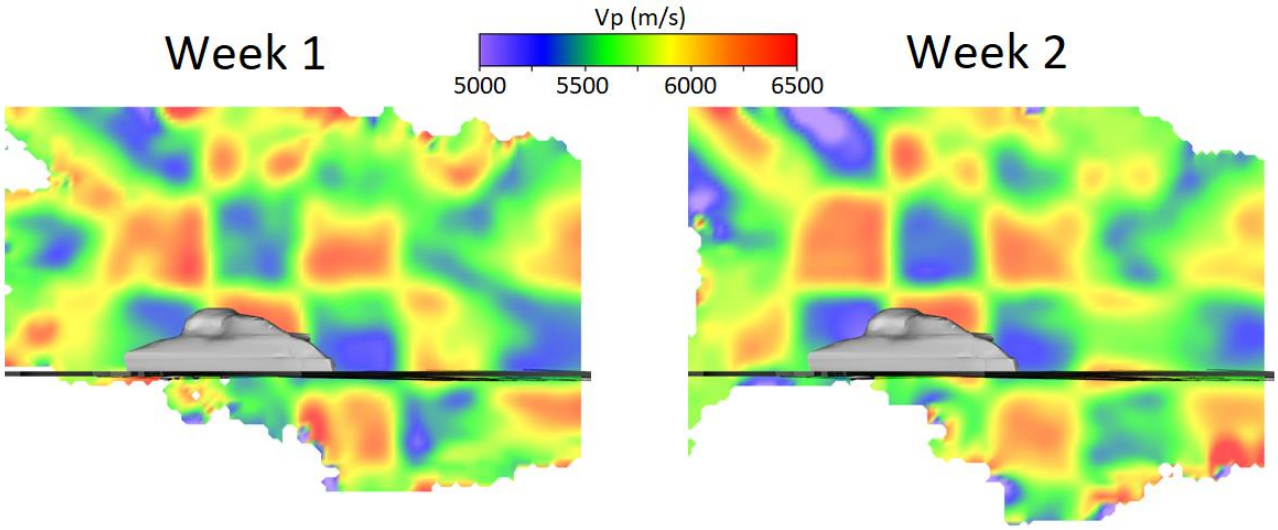

Figure 2 P-wave checkerboard test on a cross-sectional plane cutting the block cave (grey surface) for two consecutive weeks. Note the improvement in resolution in week two resulting from an increase in seismicity and the availability of more crossing ray paths. Sensor geometry remains the same in this period

2.3 Dynamic parameter analysis

It is well understood that changes in stress levels and fracture state result in the generation of microseismic events. The microseismic events can occur in close proximity and time to each other leading to finite deformation, or they can occur over larger spatial and time intervals leading to deformation on a larger scale. By analysing the collective behaviour of seismicity we can potentially identify changes in rock behaviour that occur as a result of caving operations (Figure 3). Two approaches are considered: spatial sampling and sampling based on a number of events and time differences between these events, as selected based on the characteristic space and time scales associated with operational time scales.

Several parameters are estimated for each grouping or cluster of microseismic events, such as the statistical properties of co-seismic deformation and associated changes in the strain rate, stress and rheology (see Figure 3 for a conceptual illustration of the clustering process). Specifically, we consider the time between events, the volume encompassing these events, distance between events, total time span, radiated energy, seismic moment, and density. Utilising this approach, three different behavioural identifiers (the dynamic parameters) can be defined: plasticity index (PI), stress index (SI), and diffusion index (DI). Further details on the calculation of the three indices can be found in Smith-Boughner et al. (2017).

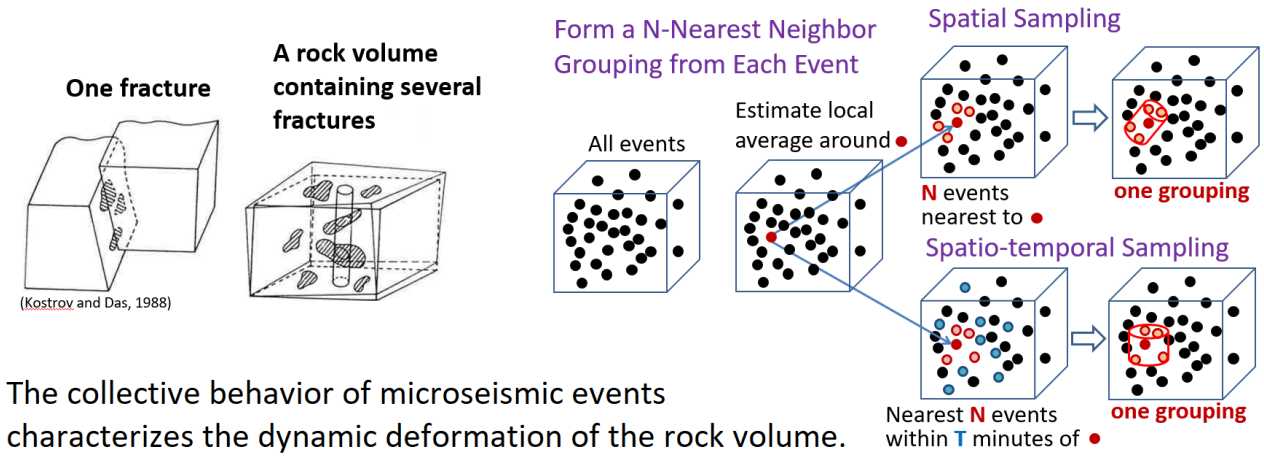

(a)

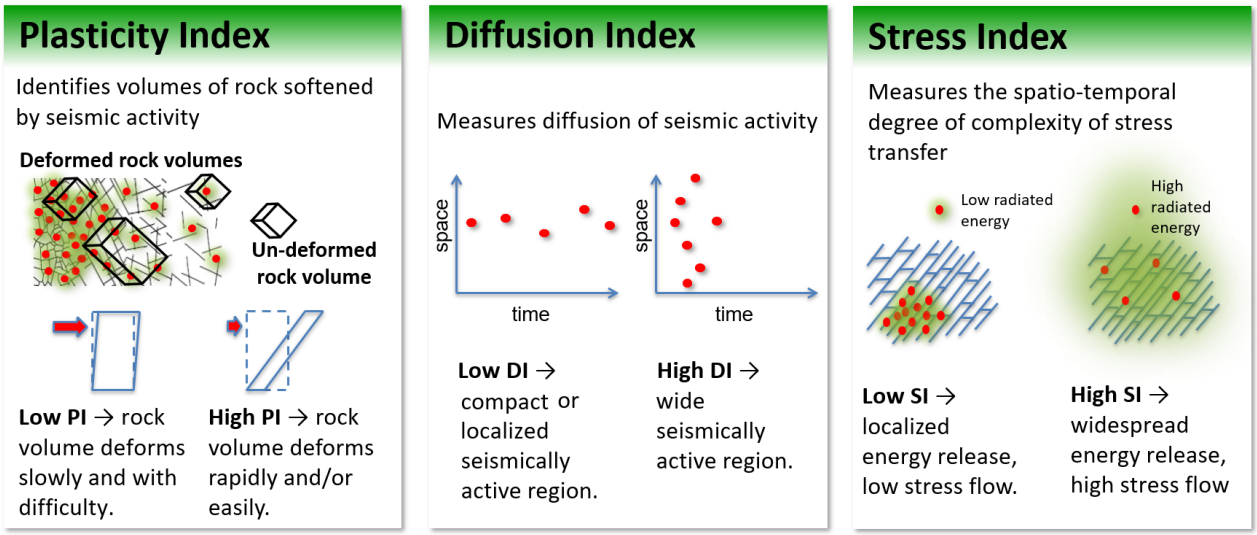

(b)

Figure 3 (a) Schematic outlining the collective behaviour of seismicity defined either by spatial or spatial-temporal clustering of events; and, (b) Schematic outlining three indices derived from the clustering approaches to describe rock behaviour

Plasticity index is used to describe the volume of rock softened by seismic activity, i.e. the deformability. As such, a low PI means the rock volume has a dominant elastic behaviour and has not suffered large amounts of deformation over time. That is, most of the seismic event energy is spent in radiation and less is spent in inelastic deformation processes. In an opposite sense, high PI clusters define rock that is easily deformable, generally related to an increase in crack complexity.

Stress index measures the ability of stress to be transferred within the rock volume through fracturing. It defines the critical state of stress within the volume and the resultant fracturing that ensues. A lower SI indicates that the transfer of stress is more unstable and localised, whereas a higher SI would indicate a less complex and further reaching stress transfer mechanism. In essence, rock volumes with localised complex fracture networks provide easier pathways to dissipate stress than a widely defined fracture network that requires a significant increase in load before failure is initiated.

Diffusion index measures the diffusion of the seismicity throughout a rock mass. It quantifies the magnitude, relative direction and velocity of the migration of seismic activity and the associated transfer of stresses in space and time. Generally, DI relates the distance between consecutive seismic events with the timing of the events and tends to migrate in space along different stress gradients. Low DI would represent seismic activity that occurs close together in space, with large inter-event times, whereas high DI would be related to events that occur in space over large inter-event distances and/or over short inter-event time intervals.

3 Data comparisons

In this study, we focused on two regions of importance to block caving: namely the cave back and the abutment. In the first instance, we consider a two-week interval and then focus on the transitions occurring over a one-month period leading to large magnitude event occurrences ($M_w > 1$). Figure 4 shows the P-wave velocity field for two consecutive weeks on a cross-sectional plane cutting the block cave (grey surface). Areas of increased P-wave velocity are observed during week one in both the cave back and the cave wall or abutment. This time interval represents a period of stress loading during cave development. Subsequent de-stressing occurred during week two, with lower velocities in both the cave back and abutment. Interestingly, there appears to be a shift with higher velocities occurring in the rock mass below the abutment. This represents a transfer of stress.

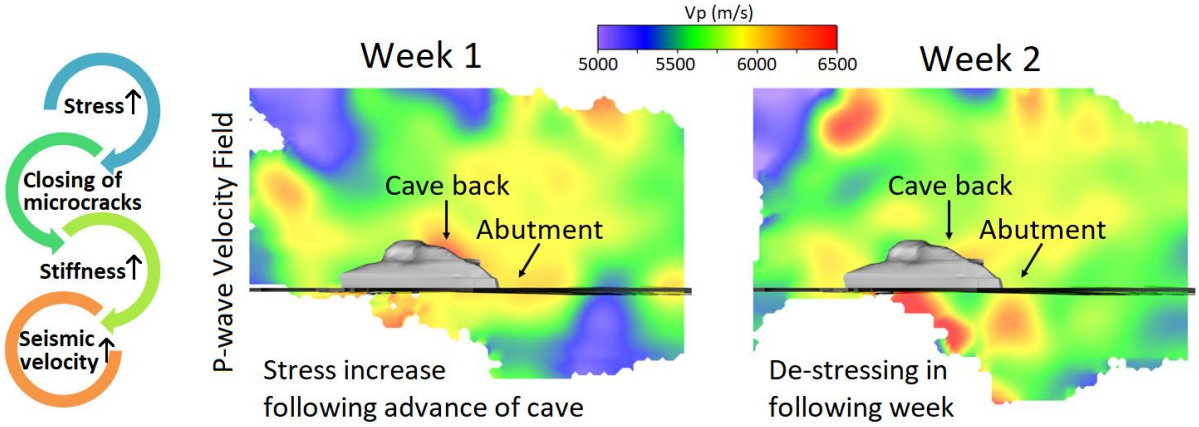

Figure 4 P-wave velocity field resulting from the tomographic inversion. The velocity field is shown relative to both the cave back and abutment for a two-week period of cave advancement

In Figure 5, the DPA is shown for the same two-week period. The three DPA fields, PI, SI and DI, are displayed over the same cross-sectional plane cutting the block cave (grey surface; as in Figure 4). An increase in the volume sampled by the dynamic parameter fields in the second week reflects an expansion of the seismically active region around the mine cave.

During the first week, we observed that the cave back region is experiencing higher deformation than the surrounding rock, as indicated by the higher PI values. However, the lower SI values suggest that the stress behaviour in the cave back is localised; in other words, energy is being released in a continuous manner. The high DI values, however, suggest that the stresses are being transferred out of the cave back region into the surrounding rock at a fairly rapid pace. During the second week, we see that the higher PI values are shifting towards the abutment. A similar observation can be made for SI, whereas DI is lower and as a result, we suggest that the stress transfer process has slowed. Based on these observations, it can be inferred that the DPA fields can provide feedback on the rock response to the cave development process.

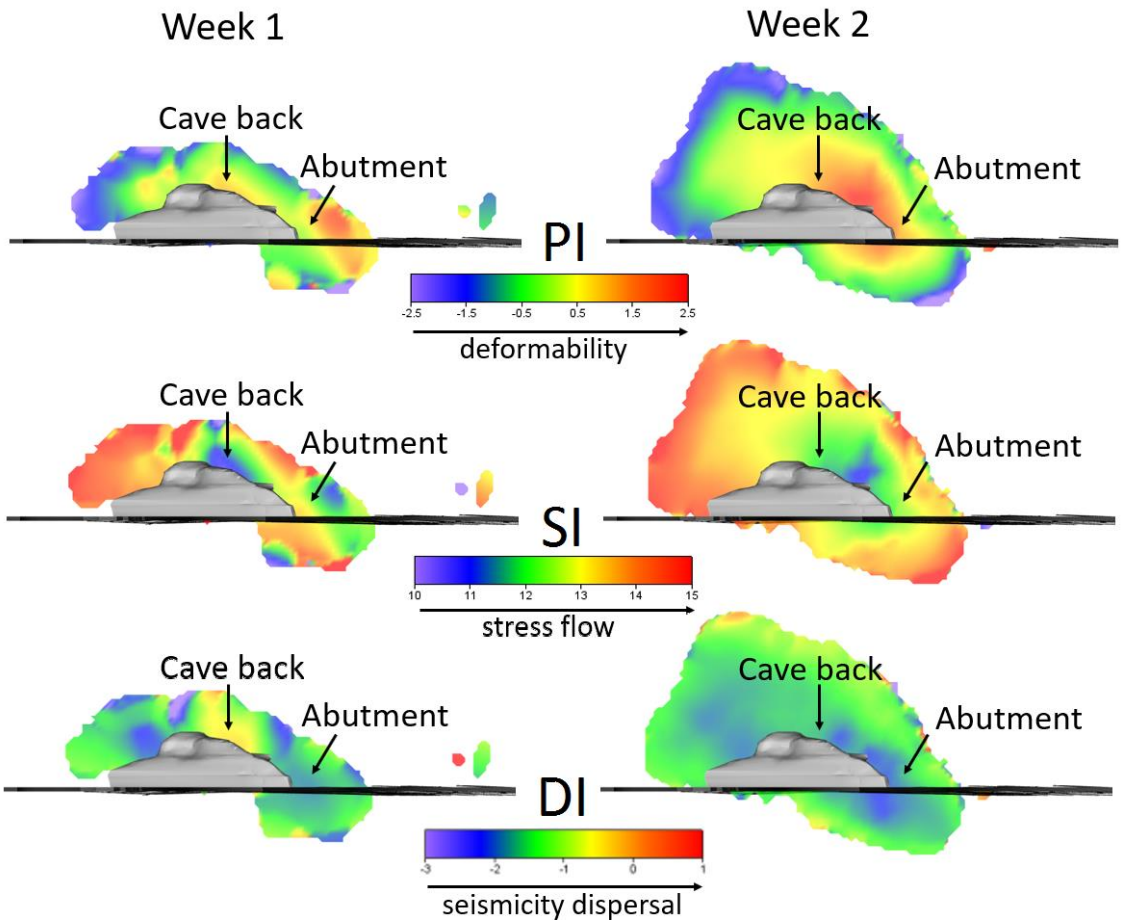

Figure 5 DPA for the same two weeks shown in Figure 4. The three DPA fields are shown over a cross-sectional plane cutting the block cave (grey surface). Results for all three DPA parameters, PI, SI and DI, are shown

If we consider the abutment region, we can similarly track changes in rock response over the two-week interval. During the first week, we observe moderate PI values or deformability in the abutment. This is accompanied by high values of SI, representing more episodic stress behaviour, or periods of increased loading. Values of DI are moderate, suggesting that the rock is not transferring stress out of the region very quickly. During week two, we see that the abutment is experiencing a large amount of deformation (high PI) under more localised stress release behaviour (lower SI and DI). Based on these observations, it could be speculated that the abutment is taking load from the cave back.

In our second example, we are considering how the velocities and collective behaviour in seismicity change over a one-month interval prior to and following three damaging events with $M_W > 1.7$ which occurred by the month's end. The partner paper to this one, de Beer et al. (2018), considers this question in more detail. We also have information on the extent of fracturing as related to the cave back from open hole data. In Figure 6, we show the distribution of seismicity as recorded over the one-month period. We also plot the event density in cross-section (same plane as used in previous example) and in plan view, with one plane through the cave and the second plane situated at the level associated with large magnitude events and damage. There is a significant level of seismicity observed throughout the entire volume surrounding the cave, with concentrations occurring at the abutments of the caving zone. As in the previous example (Figure 3), we have carried out checkerboard tests to assess the accuracy of the velocity fields determined for the site. In Figure 7, the checkerboard tests are shown for both the P- and S-wave velocities, and in both cases the velocity distributions are well-determined as compared to the initial test velocity volumes. Velocity smearing again appears to only occur away from the cave itself.

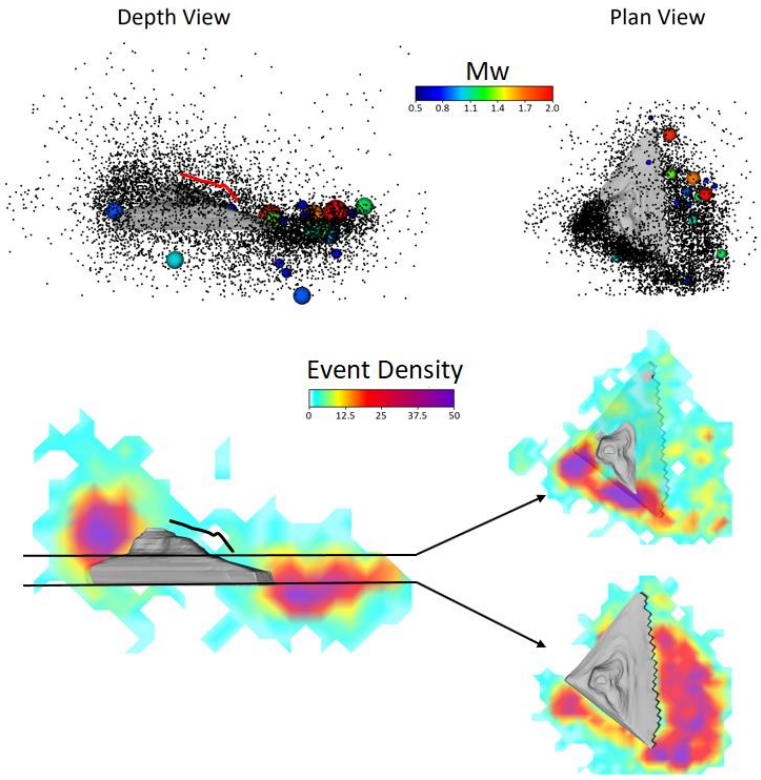

Figure 6 **Distribution in seismicity for a one-month period prior to and following the occurrence of three M_W > 1.7 events. Shown are both the events, scaled by moment magnitude, and the event density in cross-section (same view as in previous figures), and in plan view where the planes intersect the cave and the undercut level**

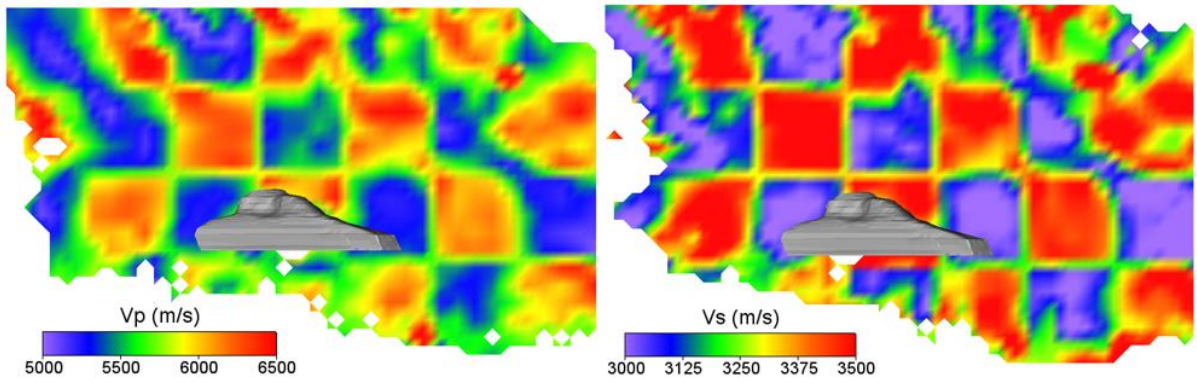

Figure 7 **P-wave and S-wave checkerboard tests on a cross-sectional plane cutting the block cave (grey surface) for the one-month data cycle prior to and following the M_w > 1.7 event occurrences**

In Figures 8 and 9, we provide both the velocity and DPA profiles along with the indicated cave back obtained by drilling during this interval. There is a high degree of correlation between the observed low P-wave velocities (lower stresses) and the inferred cave back position. Within the cave back region, the V_p/V_s ratios show that there is a difference in response next to the cave front as compared to when you move away from the front itself. The unexpected high S-wave velocities within the damaged area of the cave back may be related to stress-induced anisotropy (Nur 1969) as the direction of the maximum principal stress and the alignment of the cracks rotates around the cave and relatively to the ray propagation direction.

By considering the DPA analysis, any changes related to the cave back are diminished as compared to the behaviour within the abutments, where there is an increased level of localised deformation occurring under a relatively continuous stress release regime. Based on these observations, it can be suggested that the velocity analysis and DPA provide complementary information to understanding rock response to caving.

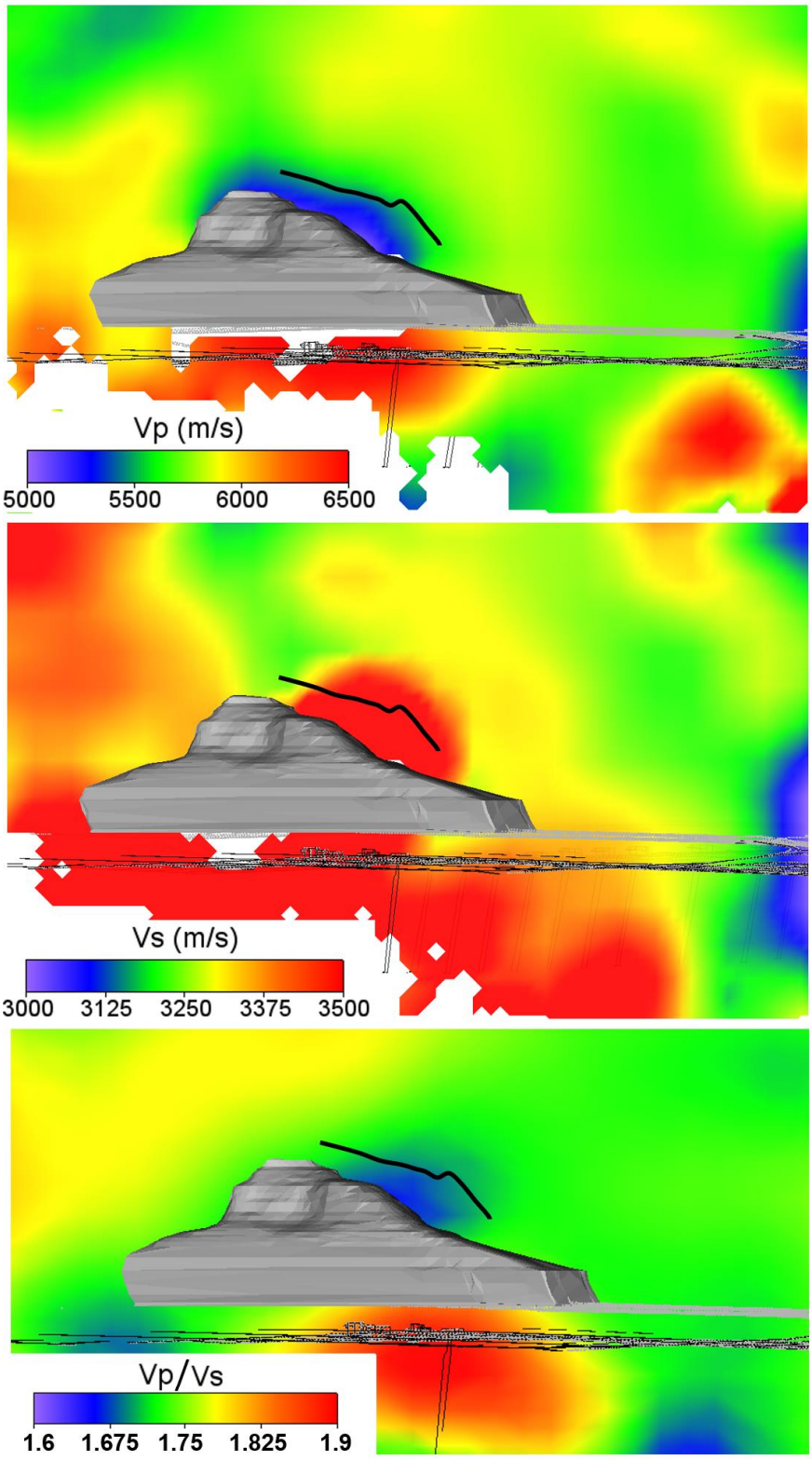

Figure 8 P-wave and S-wave velocity fields and their ratio for the one-month period

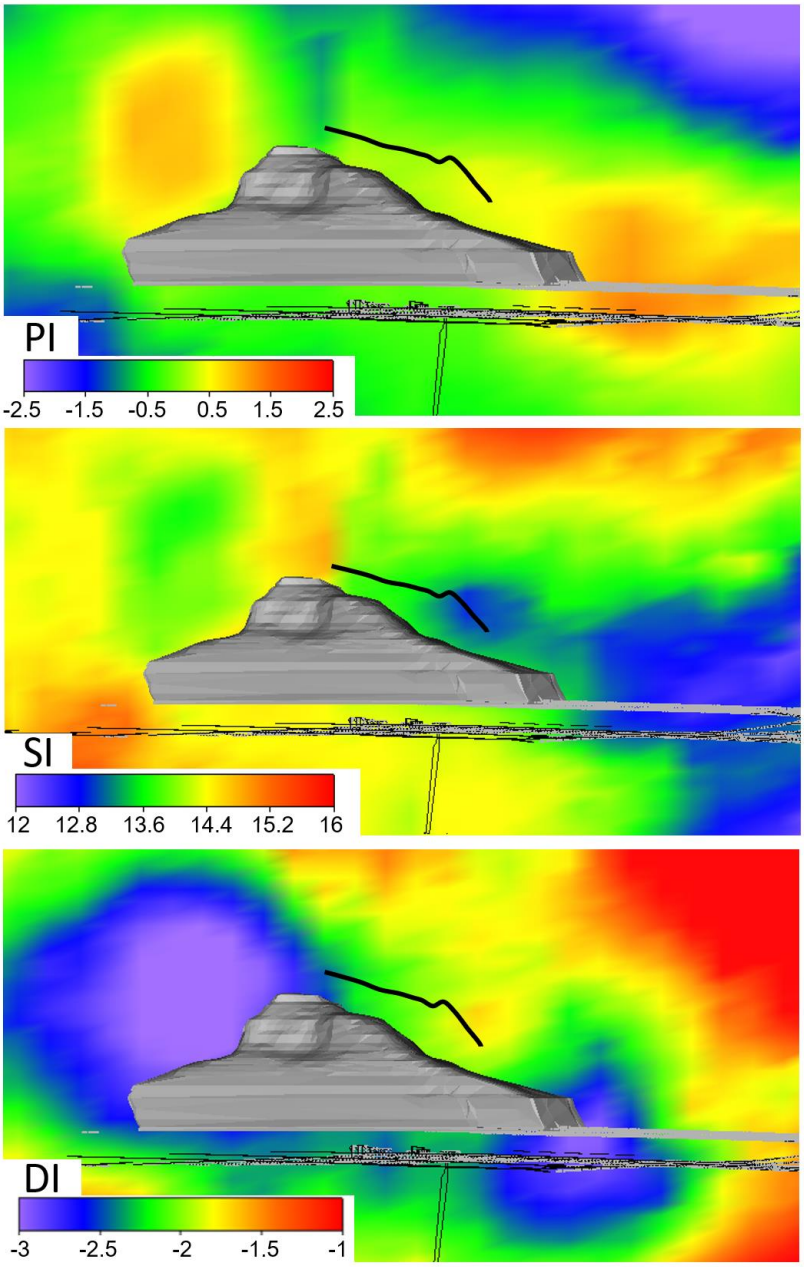

Figure 9 Dynamic parameters PI, SI, and DI for the one-month study period. Views are aligned to the velocity profiles

As shown in Figure 10, at the end of the month-long study period, a number of larger events with magnitudes ranging from M_w 1.8 to 2.1 occurred close to the cave. In Figure 11, we compare the DPA and velocity fields calculated using the one-month data with the located larger events relative to the cave in plan view, where the cutting plane is at the depth of observable damage in the vicinity of the largest events. The three largest events are not included in the DPA calculations to avoid overloading the spatial fields with the strong signal of these events in the vicinity of their location. Based on the observations, no simple or clear relationship can be found between the various fields and the location of the larger events. The three largest events ($M_W > 1.7$) occurred at the outer edge of a high-deformation area (high PI) located next to the cave front observed prior to the M_w 2.1 event (not shown). We can identify that the region surrounding the larger magnitude events ($M_w > 1.0$) during the one-month period experiences high deformation (high PI) under continuous stress release (low SI) and increasing stress (high V_p). The high V_p/V_s ratios define a corridor and the corridor is also where the large events occurred. This suggests that the corridor is behaving differently from the surrounding rock.

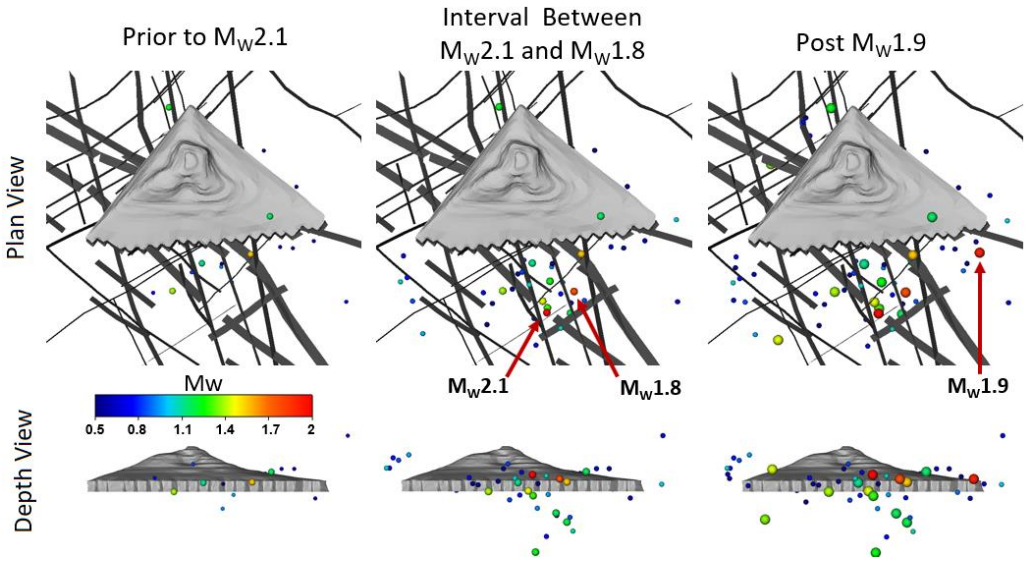

Figure 10 Distribution of seismicity with M_w > 0.5 prior to the M_w 2.1 event, the aftershock sequence (between the M_w 2.1 and 1.8 event) and post the M_w 1.9 event. Plan view is at the workings level that sustained damage in the vicinity of the M_w 2.1 event. Also indicated are the main fault sets in the vicinity of the cave

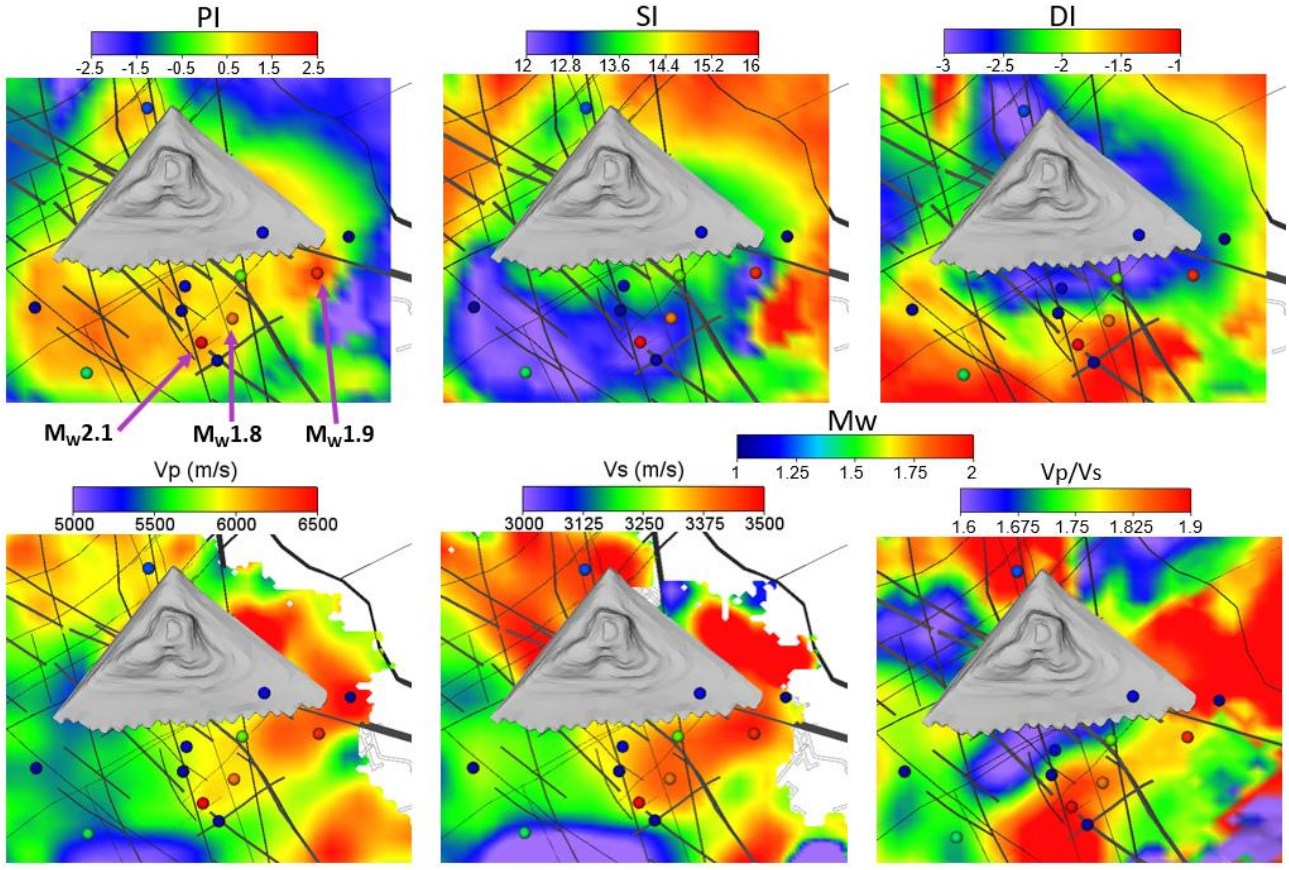

Figure 11 As in Figure 10, plan view of the DPA indices along with velocity fields. Seismicity with M_w > 1.0 above or at the field level (or working level) is also shown

4 Summary

By considering the collective behaviour of seismicity and velocity fields, a sense of how the rock is responding to caving can be identified. Based on a comparison of the velocity fields with data collected at the site, we can suggest that tracking the velocity fields provides insight into the extent of fracturing in the cave back and can be used to track those changes in time. Coupled with tracking the DPA indices, a sense of how the stresses are behaving allows operators to better understand the potential effect operations have on the rock mass in the vicinity of the caving operation itself. By combining the two approaches, a richer view of caving response is possible. However, additional studies are required to understand how these fields can be used to identify potentially hazardous locations within the mine site, although differences in velocity ratios may provide insight into the regions that may be more susceptible to catastrophic failure.

References

Ardakani, E, Baig, A, Urbancic, T & Bosman, K 2018, 'Microseismicity-derived fracture network characterization of unconventional reservoirs by topology', *Interpretation*, vol. 6, no. 2, SE49–SE61, https://dx.doi.org/10.1190/INT-2017-0172.1

Ben-Zion, Y 2008, 'Collective behavior of earthquakes and faults: Continuum-discrete transitions, progressive evolutionary changes, and different dynamic regimes', *Reviews of Geophysics*, vol. 46, no. 4, RG4006, https://dx.doi.org/10.1029/2008RG000260

Crowley, JW, Baig, A & Urbancic, T 2015, '4D tomography and deformation from microseismic data', *Proceedings of the 85th Annual Meeting of the Society of Exploration Geophysics*, Society of Exploration Geophysicists, Tulsa.

de Beer, W, Smith-Boughner, L, Viegas, G, Bosman, K & Angus, D 2018, 'Towards physics-based hazard assessment tools for developing blanket re-entry rules', in Y Potvin & J Jakubec (eds), *Proceedings of the Fourth International Symposium on Block and Sublevel Caving*, Australian Centre for Geomechanics, Perth, pp. 573–580.

Kostrov, BV & Das, S 1988, *Principles of Earthquake Source Mechanics*, Cambridge University Press, Cambridge.

Ma, X, Westman, EC, Fahrman, BP & Thibodeau, D 2016, 'Imaging of temporal stress redistribution due to triggered seismicity at a deep nickel mine', *Geomechanics for Energy and the Environment*, vol. 5, pp. 55–64.

Mercier, J-P, de Beer, W, Mercier, J-P & Morris, S 2015 'Evolution of a block cave from time-lapse passive source body-wave traveltime tomography', *Geophysics*, vol. 80, no. 2, pp. WA85–WA97, https://dx.doi.org/10.1190/geo2014-0155.1

Nolet, G 2008, *A Breviary of Seismic Tomography*, Cambridge University Press, Cambridge.

Nur, A & Simmons, G 1969, 'Stress-induced velocity anisotropy in rock: An experimental study', *Journal Geophysical Research*, vol. 74, no. 27, pp. 6667–6674, https://dx.doi.org/10.1029/JB074i027p06667

Rawlinson, N & Sambridge, M 2003, 'Seismic traveltime tomography of the crust and lithosphere', *Advances in Geophysics*, vol. 46, pp. 81–198.

Riznichenko, YV 1965, 'Seismic rock flow', *Dynamics of the Earth's Crust*, Nauka, Moskow, in Russian.

Smith-Boughner, L, Urbancic, T & Baig, A 2017, 'Resolving sill pillar stress behavior associated with blasts and rockbursts', in J Wesseloo (ed.), *Proceedings of the Eighth International Conference on Deep and High Stress Mining,* Australian Centre for Geomechanics, Perth, pp. 257–267.

Urbancic, T, Smith-Boughner, L, Crowley, JW, Viegas, G, Baig, A & von Lunen, E 2015, 'Characterizing the dynamic growth of a fracture network', *Proceedings of the Unconventional Resources Technology Conference*, Society of Petroleum Engineers, Richardson, http://dx.doi.org/10.15530/URTEC-2015-2154641

Westman, E, Luxbacher, K & Schafrik, S 2012, 'Passive seismic tomography for three-dimensional time-lapse imaging of mining-induced rock mass changes', *The Leading Edge*, vol. 31, pp. 338–345.